

## Demonstration of Saturation in a Ni-like Ag X-Ray Laser at 14 nm

J. Zhang,<sup>1,\*</sup> A. G. MacPhee,<sup>2</sup> J. Nilsen,<sup>3</sup> J. Lin,<sup>4</sup> T. W. Barbee, Jr.,<sup>3</sup> C. Danson,<sup>5</sup> M. H. Key,<sup>3</sup> C. L. S. Lewis,<sup>2</sup> D. Neely,<sup>5</sup> R. M. N. O'Rourke,<sup>2</sup> G. J. Pert,<sup>6</sup> R. Smith,<sup>4</sup> G. J. Tallents,<sup>4</sup> J. S. Wark, and E. Wolfrum<sup>1</sup>

<sup>1</sup>Clarendon Laboratory, Department of Physics, University of Oxford, Oxford, OX1 3PU, United Kingdom

<sup>2</sup>School of Mathematics and Physics, Queen's University of Belfast, Belfast, BT7 1NN, United Kingdom

<sup>3</sup>Lawrence Livermore National Laboratory, Livermore, California 94550

<sup>4</sup>Department of Physics, University of Essex, Colchester, CO4 3SQ, United Kingdom

<sup>5</sup>Central Laser Facility, Rutherford Appleton Laboratory, Chilton, Oxon OX11 0QX, United Kingdom

<sup>6</sup>Department of Physics, University of York, York, YO1 5DD, United Kingdom

(Received 30 December 1996; revised manuscript received 24 February 1997)

We report the first demonstration of saturation in a Ni-like x-ray laser, specifically Ni-like Ag x-ray laser at 14 nm. Using high-resolution spatial imaging and angularly resolved streaking techniques, the output source size as well as the time history, divergence, energy, and spatial profile of the output beam have been fully characterized. The output intensity of the Ag laser was measured to be about 70 GW cm<sup>-2</sup>. The narrow divergence, short pulse duration, high efficiency, and high brightness of the Ag laser make it an ideal candidate for many x-ray laser applications. [S0031-9007(97)03079-2]

PACS numbers: 42.55.Vc

Saturation has been observed in Ne-like x-ray lasers on the  $J = 2 \rightarrow 1$  transitions in plasmas of Ge [1], Se [2], and Y [3] and on the  $J = 0 \rightarrow 1$  transition in Zn [4], Ar [5], Ge [6], and Ti [7] plasmas. Saturated operation is very important because it means that the maximum power possible for a given volume of excited plasma is extracted by the stimulated emission. Saturation also tends to produce an output sufficient for applications and ensures the production of a consistent output with little variation from shot to shot. Such saturated x-ray lasers at shorter wavelengths are required for holography, microscopy, interferometry, radiography, and many other applications [8–11].

Although Ne-like x-ray lasers have shown large gains and gain length products, they are difficult to scale to the shorter wavelengths required for most applications, with the currently available laser driver energy. Ni-like x-ray lasers, in principle, work at much shorter wavelengths for the same amount of driver energy but have difficulties to provide saturated output. There have been significant achievements in developing Ni-like x-ray lasers at shorter wavelengths [12,13]. Recent experiments have shown that the intensity and the efficiency of Ni-like x-ray lasers can be greatly enhanced by the use of multiple equal intensity short pulses with 400 ps intervals [14–18]. A significant gain-length product of  $\sim 8$  has been reported [15,17], which, however, is still too low for saturated operation.

In the multipulse mode, the first pulse heats and ionizes the plasma but the density gradients are too steep for laser propagation. The plasma then expands creating a larger scale length plasma and produces a larger, more uniform gain region which allows for good laser propagation [19–21]. Aiming at improving efficiency and enhancing the gain-length product, we used a different drive pulse configuration compared to previous Ni-like

experiments carried out by other groups [15–17]. Since it is not necessary to have a preplasma in an ionization stage as high as Ni-like, a low intensity ( $\sim 10\%–30\%$  of total energy) laser pulse (prepulse) was used to create a preplasma with a lower ionization. The preplasma was then allowed to cool down for a much longer time ( $>2$  ns) than those used in other experiments [15–17], until it became not as transparent to the following laser pulse (main pulse) and the plasma region, where laser gain generates, can directly absorb more energy from the main laser pulse before it hits the critical density surface of the plasma. A larger separation ( $>1$  ns) between the prepulse and main pulse produces a larger gain region with lower gradients which allows for better propagation and therefore higher laser output [6,22]. In this Letter, we present the first demonstration of saturation in a Ni-like x-ray laser, specifically, the Ni-like Ag laser at 14 nm from a refraction compensating double target.

The experimental setup is similar to that described in Ref. [6]. Three beams of the VULCAN Nd:glass laser with a 75 ps pulse duration at 1.05  $\mu\text{m}$  were used in a standard off-axis focus geometry, which provide a line focus with 25 mm length and 200  $\mu\text{m}$  width, giving an irradiance of  $\sim 20$  TW cm<sup>-2</sup> on targets. Deploying the other three beams 180° opposed in a second line focus produced a plasma with an opposed density gradient which helps compensate for the refraction of the x-ray laser beam from the first plasma.

Flat slab targets used in the experiment were typically 18 mm long with 200  $\mu\text{m}$  wide Ag stripes coated on the glass substrates. For some shots, targets with 20 or 22 mm length were used for gain measurements. Both ends of the slab target were placed well within the line focus to avoid cold plasmas at the ends of the targets. The targets were aligned so that they were parallel with an adjustable separation (in the direction perpendicular to the

target surfaces) between the surface planes and an axial separation of  $500 \mu\text{m}$  between the two targets. For some shots, curved targets with a  $100 \text{ cm}$  radius of curvature were used to make a comparison with the performance of flat slab targets. Since the x-ray laser pulse duration is comparable to the propagation time, traveling wave excitation for the two successive targets is desirable to achieve maximum amplification. To approximate this condition, the three drive beams for the first slab target were therefore timed  $60 \text{ ps}$  earlier than the three beams for the second target.

The primary diagnostics along the target axis were two flat-field grazing incidence x-ray spectrometers with  $1200 \text{ lines/mm}$  aperiodically ruled gratings [6]. They recorded the spectral range from  $5.0$  to  $30.0 \text{ nm}$  on InstaSpec IV back-thinned soft x-ray CCD detectors (Oriental Instruments, Stratford, CT). Radiation at wavelengths shorter than  $6.0 \text{ nm}$  was eliminated by the use of two parallel Ag mirrors at  $10^\circ$  grazing incidence angle. Si and C filters were used to provide variable attenuation and absorption edges for wavelength calibration. The axial spectra in a given axial direction were recorded in either of two ways. Time averaged spectra with angular resolution were obtained using an x-ray CCD detector in the focal plane. Alternatively, the Ag laser line at  $14 \text{ nm}$  was focused by the grating of an axial flat field spectrometer into the entrance of a streak camera so that the streak displayed the temporal variation of the angular distribution of the Ag laser line [1]. The laser line width was less than  $50 \mu\text{m}$  at the streak entrance plane so the temporal resolution is limited by the streak camera operation to  $\sim 10 \text{ ps}$ . A fiber-optic coupled CCD detector (Oriental Instruments) recorded the time-resolved angular distribution.

In order to measure the output energy and the spatial profile of the Ag x-ray laser, a near field imaging diagnostic [6,23,24] was used consisting of multilayer mirrors, Al and C filters and an x-ray CCD detector. The two mirrors had a combined measured peak reflectivity of about  $20\%$  at a central wavelength  $14 \text{ nm}$  with a full width at half maximum (FWHM) bandwidth around  $1.0 \text{ nm}$ . The concave multilayer mirror had  $25 \text{ cm}$  focal length and was positioned to image the output end of the Ag x-ray laser which was relayed off a  $45^\circ$  planar multilayer mirror onto the x-ray CCD detector at a magnification of  $22\times$ .

Figure 1 shows the measured time integrated on-axis output spectrum from a  $18 \text{ mm}$  long single curved target. The output is completely dominated by the Ni-like Ag  $J = 0 \rightarrow 1$  laser transition at  $14 \text{ nm}$  and its second order. The intensity of the laser line was attenuated by a combination of Si and C filters by a factor of  $100$  to avoid saturation of the CCD detector. There are a few tenths of a nm uncertainty in the measured wavelength of the laser line. This line was predicted to be at  $14.0 \text{ nm}$  [25].

Figure 2 presents streak images showing the temporal behavior of the angular distribution in the exit plane

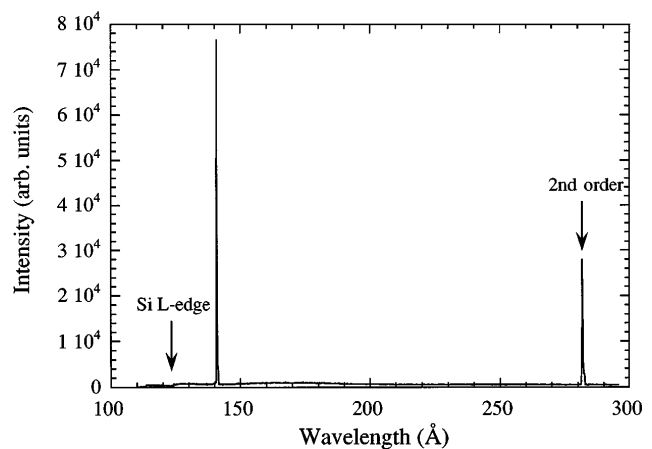


FIG. 1. Axial spectrum from a  $18 \text{ mm}$  long single curved Ag target showing that the  $14\text{-nm}$  laser line and its second order completely dominate the spectrum. The laser line has been attenuated by a factor of  $100$  to avoid saturation of the CCD detector.

perpendicular to the target surface of the Ag laser from a single flat target, a coupled double flat target with an optimized separation of  $150 \mu\text{m}$  and from a single curved target. The grey levels of the three graphs were normalized to the same level to show the angular and temporal distributions for the different target geometries. The peak emission from the double target is about  $200$  times stronger than the emission from a single flat target and about  $80$  times stronger than that from a curved target. The laser emission from the single target has a broad divergence of  $3.4 \text{ mrad}$  and peaks at  $4.5 \text{ mrad}$  off axis. It lasts about  $34 \text{ ps}$ . By comparison, the laser emission from a coupled double target shows a strong coupling effect both angularly and temporally. Its pulse duration

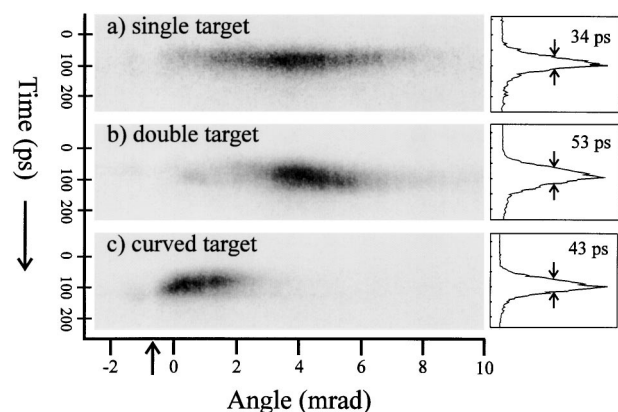


FIG. 2. Typical x-ray streak images of angular distributions of the Ni-like Ag  $14 \text{ nm}$  laser line from (a) a single flat target, (b) a double flat target with a perpendicular separation of  $150 \mu\text{m}$ , and (c) a single curved target with  $100 \text{ cm}$  radius of curvature. At the right-hand side are the temporal traces. The arrow at the bottom indicates the fiducial wire at  $-0.5 \text{ mrad}$  from the target surface.

is somewhat longer due to the contribution from two targets and its divergence is 2.1 mrad. The emission from a curved target has the smallest divergence ( $\sim 1.7$  mrad) and peaks at only 0.8 mrad from the target surface. The pulse duration from the curved target is about 43 ps. It is apparent that the angle of the laser beam from the curved target sweeps in time towards the target surface. The angle of the peak intensity is influenced by refraction of the beam in the plasma. The pulse durations shown in Fig. 2 are single scans through the angular peaks of the laser emission. The angularly integrated durations are somewhat longer.

The output intensity of the Ag laser is plotted in Fig. 3 against plasma length. For those single target plasmas with lengths  $< 22$  mm, the increase in output intensity of the laser line is a simple exponential form. The gain coefficient was determined by fitting the Linford formula to those data in the exponential region, to be  $7.2 \pm 0.4 \text{ cm}^{-1}$ . The output intensity no longer increases exponentially with the plasma length for targets longer than 22 mm, beyond which the gain-length product is greater than 16 and the output intensity increases linearly and varies little from shot to shot.

Images of the spatial distribution of the Ag laser at the output aperture of the Ag laser from single, double, and curved slab targets were recorded to study the laser output pattern and mode structure. The characteristics at the near field of a single flat target and double flat target were similar to those observed at near field of the Ne-like Ge  $J = 0 \rightarrow 1$  laser [6]. The output aperture of the Ag laser from a curved target was, however, smaller. Figure 4 shows the near field image from a double flat Ag target with a perpendicular separation of  $150 \mu\text{m}$ . The horizontal axis in the figure is the expansion direction perpendicular to the target surface and the vertical axis

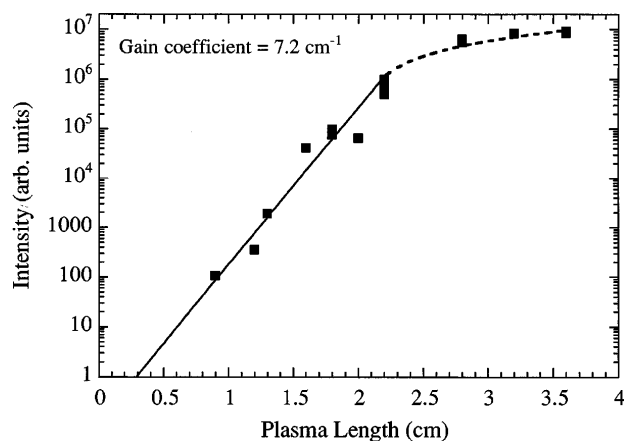


FIG. 3. Peak intensity as a function of plasma length. The solid line shows exponential increase of the output intensity and the broken line shows the linear increase in the saturation region. Saturation is reached at an approximate gain-length product of 16.

parallel to the target surface. The VULCAN laser beams are incident from left and right, respectively, on the two targets, with the line foci along the line of sight (out of the page). The target surface position was determined using the peak of the thermal emission from the target surface. The individual contributions from both targets are visible at the left and bottom part of the image. Most of the energy is concentrated in the coupled region. The FWHM extent in the transverse direction is about  $43 \mu\text{m}$ . In the perpendicular direction, there is much structure in the laser pattern. The beam pattern peaks in the region around  $150 \mu\text{m}$  from the target surface.

Since the collection solid angle of the multilayer mirror system overfills the angular distribution of the Ag laser beam, the output intensity can be estimated by integrating the total photons emitted from the output aperture and using an absolute calibration for the CCD detector, the calibrations for the x-ray multilayer mirrors, filters, and the measured angularly integrated x-ray laser pulse duration. The output intensity of the Ag laser for an optimized separation ( $150 \mu\text{m}$ ) between the two targets was estimated to be  $\sim 90 \mu\text{J}$ , corresponding to a conversion efficiency of  $6 \times 10^{-7}$ , which is the highest efficiency achieved for Ni-like x-ray lasers. The maximum intensity of the Ag laser is about  $69 \text{ GW cm}^{-2}$ . The estimated uncertainty in this measurement is a factor of 1.5 and is due predominantly to uncertainty in the filter attenuation. Given our best estimates of the source size ( $43 \times 57 \mu\text{m}^2$ ), and the beam divergence (1.5 mrad perpendicular by 3.5 mrad parallel), a brightness of  $1.1 \times 10^{25} \text{ photons s}^{-1} \text{ mm}^{-2} \text{ mrad}^{-2}$  is calculated. It is of interest to compare the output intensity

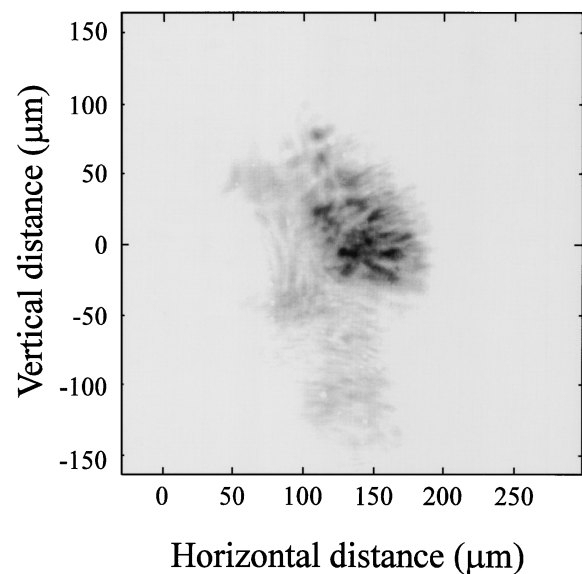


FIG. 4. The end-on view of the Ni-like Ag x-ray laser from a coupled double target with a separation of  $150 \mu\text{m}$ . The zero position on the horizontal axis is the target surface while the zero position on the vertical axis shows the center of the line focus on the target.

of the Ag laser with the saturated intensity estimated from the Einstein relations between spontaneous and stimulated emission [3,6]. The decay rate of the upper laser level is calculated from XRASER [26] kinetic simulations to be  $6.31 \text{ ps}^{-1}$  and the spontaneous emission rate of the upper laser level to the lower is  $0.215 \text{ ps}^{-1}$ . Most of the upper level destruction rate is due to collisional mixing. The total destruction rate of the lower laser level is  $7.46 \text{ ps}^{-1}$ . In the simulations, typical plasma conditions for the Ag laser were used: an electron temperature of 700 eV, and an electron density of  $5.7 \times 10^{20} \text{ cm}^{-3}$ . The saturated intensity is then calculated to be  $28 \text{ GW cm}^{-2}$ , which is about one third of the measured value. It should be noted that the saturation intensity is not an upper bound on the output but just the starting point at which the energy extraction becomes efficient for the laser operation.

In conclusion, we have demonstrated the first saturated Ni-like x-ray laser using only about  $20 \text{ TW cm}^{-2}$  intensity on target, that is, a focused intensity which can be achieved by many other smaller scale laser facilities. The narrow divergence, short pulse duration, high efficiency, and high brightness of the Ag laser make it an ideal candidate for many x-ray laser applications. Using the available energies of the VULCAN laser on a narrower line focus, saturated output in Ni-like x-ray lasers can be achieved at much shorter wavelengths. This is an important step towards saturated operation of x-ray lasers at the water window.

This work is part of a programme on x-ray laser research funded by EPSRC under Grants No. GR/L 11540, No. 11946, No. 11779, and No. 11809. E.W. has been supported by the Austrian Fonds zur Förderung der wissenschaftlichen Forschung under Project No. P10844 NAW. The work of the LLNL authors was performed under the auspices of the U.S. Department of Energy by the Lawrence Livermore National Laboratory under Contract No. W-7405-Eng-48.

\*To whom correspondence should be addressed at Central Laser Facility, Rutherford Appleton Laboratory, Chilton, DIDCOT, OX11 0QX, UK.

Electronic address: J.Zhang@rl.ac.uk

- [1] A. Carillon *et al.*, Phys. Rev. Lett. **68**, 2917 (1992); S. Wang *et al.*, Sci. China A **34**, 1388 (1991).
- [2] J. A. Koch *et al.*, Phys. Rev. Lett. **68**, 3291 (1992).
- [3] L. B. Da Silva *et al.*, Opt. Lett. **18**, 1174 (1993).
- [4] P. Jaegle *et al.*, in *X-ray Lasers—1994*, AIP Conf. Proc. No. 332 (AIP, New York, 1994), p. 25.
- [5] J. J. Rocca *et al.*, Phys. Rev. Lett. **77**, 1476 (1996).
- [6] J. Zhang *et al.*, Phys. Rev. A **54**, R4653 (1996).
- [7] P. V. Nickles *et al.* (to be published).
- [8] J. E. Trebes *et al.*, Science **238**, 517 (1987).
- [9] L. B. Da Silva *et al.*, Phys. Rev. Lett. **74**, 3991 (1995).
- [10] D. H. Kalantar *et al.*, Phys. Rev. Lett. **76**, 3574 (1996).
- [11] A. S. Wan *et al.*, Proc. Soc. Photo-Opt. Instrum. Eng. **2520**, 268 (1995).
- [12] B. J. MacGowan *et al.*, Phys. Fluids B **4**, 2326 (1992).
- [13] C. L. S. Lewis *et al.*, *X-Ray Lasers—1992*, edited by E. E. Fill, IOP Conf. Proc. No. 125 (Institute of Physics and Physical Society, London, 1992), p. 23.
- [14] S. Basu *et al.*, Appl. Phys. B **57**, 303 (1993).
- [15] H. Daido *et al.*, Phys. Rev. Lett. **75**, 1074 (1995).
- [16] J. Nilsen and C. Moreno, Opt. Lett. **20**, 1387 (1995).
- [17] H. Daido *et al.*, Opt. Lett. **21**, 958 (1996).
- [18] Y. Li *et al.*, Phys. Rev. A **53**, R652 (1996).
- [19] J. Nilsen and J. C. Moreno, Phys. Rev. Lett. **74**, 337 (1995).
- [20] J. Zhang *et al.*, Phys. Rev. A **53**, 3640 (1996).
- [21] J. Nilsen *et al.*, Phys. Rev. A **55**, 827 (1997).
- [22] J. Zhang *et al.* (to be published).
- [23] G. Cairns *et al.*, Appl. Phys. B **58**, 51 (1994).
- [24] J. Zhang *et al.*, Phys. Rev. Lett. **74**, 1335 (1995).
- [25] J. H. Scofield and B. J. MacGowan, Phys. Scr. **46**, 361 (1992).
- [26] J. Nilsen, in *Radiative-Hydro Modeling and Atomic Data Bases*, edited by Allan Hauer and A. L. Merts, AIP Conf. Proc. No. 168 (American Institute of Physics, New York, 1988), pp. 51–58.